Environ Geol (2007) 52:965–977
DOI 10.1007/s00254-006-0539-z

ORIGINAL ARTICLE

Reactions and reaction rates in the regional aquifer beneath the Pajarito Plateau, north-central New Mexico, USA

Anne G. Hereford · Elizabeth H. Keating · George D. Guthrie Jr · Chen Zhu

Received: 17 July 2006 / Accepted: 26 September 2006 / Published online: 10 November 2006

Abstract Reactions and reaction rates within aquifers are fundamental components of critical hydrological processes. However, reactions simulated in laboratory experiments typically demonstrate rates that are much faster than those observed in the field. Therefore, it is necessary to conduct more reaction rate analyses in natural settings. This study of geochemical reactions in the regional aquifer in the Pajarito Plateau near Los Alamos, New Mexico combines modeling with petrographic assessment to further knowledge and understanding of complex natural hydrologic systems. Groundwater geochemistry shows marked evolution along assumed flow paths. The flow path chosen for this study was evaluated using inverse mass balance modeling to calculate the mass transfer. X-ray diffraction and field emission gun scanning electron microscopy were used to identify possible reactants and products. Considering the mineralogy of the aquifer and saturation indices for the regional water refined initial interpretations. Calculations yielded dissolution rates for plagioclase on the order of 10^{-15} mol s^{-1} m^{-2} and for K-feldspar on the order of 10^{-17} mol s^{-1} m^{-2}, orders of magnitude slower than laboratory rates. While these rates agree with other aquifer studies, they must be considered in the light of the uncertainty associated with geometric surface area estimates, ^{14}C ages, and aquifer properties.

A. G. Hereford · C. Zhu (✉)
Department of Geological Sciences, Indiana University,
Bloomington, IN 47405, USA
e-mail: chenzhu@indiana.edu

E. H. Keating · G. D. Guthrie Jr
Los Alamos National Laboratories,
Los Alamos, NM 87545, USA

Keywords Feldspar · Inverse mass balance modeling · USA · Geochemistry · Kinetics

Introduction

Water–rock reactions and reaction rates in aquifers are fundamental components of critical hydrological processes. However, silicate dissolution reactions simulated in laboratory experiments demonstrate rates that are up to five orders of magnitude faster than those found in natural settings (Paces 1983; Velbel 1985, 1990; Brantley 1992; Blum and Stillings 1995; Drever and Clow 1995; White et al. 2001; White and Brantley 2003; Zhu 2005). Generally, being able to accurately model water–rock interactions in the sub-surface is critical to many geological and environmental problems including water quality and contaminant transport; the role of feldspar dissolution in the process of carbon sequestration; and the possible relationship between weathering and global climate change through geologic time. Numerous field studies of unsaturated zone and small watershed systems have been reported (see references above), but these systems are complex (Alsaaran and Olyphant 1998) and their processes are not directly applicable to larger systems. While aquifers are major sites for water–rock interactions and present some advantages over studying in situ rates in soil profiles and streams (Zhu 2005), there is a paucity of studies of reaction rates in aquifers. Understanding the reactions that are taking place in an aquifer will allow for the use of the water chemistry as a natural tracer in the aquifer and will improve detection of the migration of reactive contaminants in the system (Keating and Warren 1999).

The regional aquifer in the vicinity of the Pajarito Plateau is a natural choice for this type of study. The large amount of hydrological and geochemical data collected in the last four decades (Griggs 1964; Mcada and Wasiolek 1988; Blake et al. 1995; Rogers et al. 1996; Keating and Bahr 1998; Keating and Warren 1999; Broxton and Vaniman 2005; Keating et al. 2005; Newman and Robinson 2005) allows for a more thorough assessment of in situ reactions and reaction rates. Available studies include chemical analyses of groundwater samples (Blake et al. 1995), ^{14}C ages for aquifer waters (Rogers et al. 1996), flow models of the regional aquifer (Mcada and Wasiolek 1988; Keating et al. 2005), and X-ray diffraction (XRD) analyses (Keating and Warren 1999). The variety of data available affords an opportunity to crosscheck model-inferred reactions and reaction rates with local mineralogy and geochemistry.

This study presents model-based in situ reaction rate estimates for the regional aquifer in the vicinity of the Pajarito Plateau. The mass transfer between groundwater and solid matrix were estimated using the inverse mass-balance modeling approach (Garrels and Mackenzie 1967; Plummer and Back 1980, 1983, 1994). The travel times between wells were estimated from ^{14}C data (Rogers et al. 1996). A scanning electron microscope (SEM) was used to characterize the mineral phases and mineral textural relationships in the aquifer matrix. The reaction rates derived in this study should help in predicting rates in other sandy aquifers.

Geology, hydrology, and geochemistry

The study area is in the west-central portion of the Española Basin in north-central New Mexico (Fig. 1). The Basin is a north- to north-west trending syncline and is part of the Rio Grande depression (one of the basins of the Basin and Range Province) (Mcada and Wasiolek 1988). The Española Basin is bounded to the east by the Sangre de Cristo Mountains and to the west by the Jemez Mountains. The primary aquifers in this region are sedimentary units, with some volcanic units being locally significant as perched aquifers (Griggs 1964). Pumping wells in the Pajarito Plateau supply water to Los Alamos National Laboratory (LANL) and to the towns of Los Alamos and White Rock. Most are calcium bicarbonate waters; some northeast of Los Alamos are sodium bicarbonate (Frenzel 1995).

The aquifer under consideration is primarily in the Tesuque, Chamita, and lower Puye formations of the Santa Fe Group. The Tesuque is a series of alluvial fan deposits that originated from points north and east. The formation has a dip of 4–10° to the west, with the steeper dips being found in the eastern portion of the Pajarito Plateau (Frenzel 1995). The Chamita and lower Puye formations include some sections of coarser, high-yielding, higher permeability sediments, which Purtymun (1995) considers to be deposits of the ancestral Rio Grande. While the majority of the recharge to the aquifer originates in the mountains along the western edge of the basin, up to 14% may derive from losing streams; over most of the plateau, recharge must pass through the Bandelier Tuff, and other volcanics en route to the aquifer (Keating et al. 2005). Furthermore, the plateau, at approximately 2,500 m elevation, has a high evaporation rate, and does not receive much precipitation; thus local recharge is a small percentage of the total. The aquifer discharges to the Rio Grande at approximately 1,675 m elevation, and possibly into the adjacent basin to the south at depth (Keating et al. 2005). There are no available data that suggest flow has deviated from the same east to southeast path for the past several thousand years (Keating et al. 2005). Groundwater flow is now affected by pumping, which began circa 1950.

The water table in the aquifer ranges from approximately 365 m below the ground surface just west of LANL to 180 m at the eastern margin of the plateau (Rogers et al. 1996). The land surface also slopes down to the east, resulting in a net change of approximately 300 m in the elevation of the water table.

Models were based on data from one spring and three wells progressing from the Pajarito Plateau to the plains of the Rio Grande. The flow path connecting these points is approximately 16.3 km long, with the first segment being 6,850 m, the second 2,900 m and the third 6,500 m. The data collection sites were chosen to represent the evolution of groundwater as it travels from the Jemez Mountains to the Rio Grande, but are not necessarily on an exact flow path. The sites were selected because they are considered to be representative of the chemical evolution seen in the plateau waters and because they are aligned with the presumed flow direction perpendicular to water table contours (Keating and Warren 1999). As discussed in Keating and Warren (1999), Pine Spring is assumed to be sourced from a perched aquifer and to be representative of the water recharging the regional aquifer in the Sierra del los Valles. This recharge water is slightly acidic and has low total dissolved solids (TDS). TDS and pH increase along the hypothetical flow path, TDS from 126 to 310.5 mg/kg; pH from 5.5 to 8.9. Changes in TDS, pH

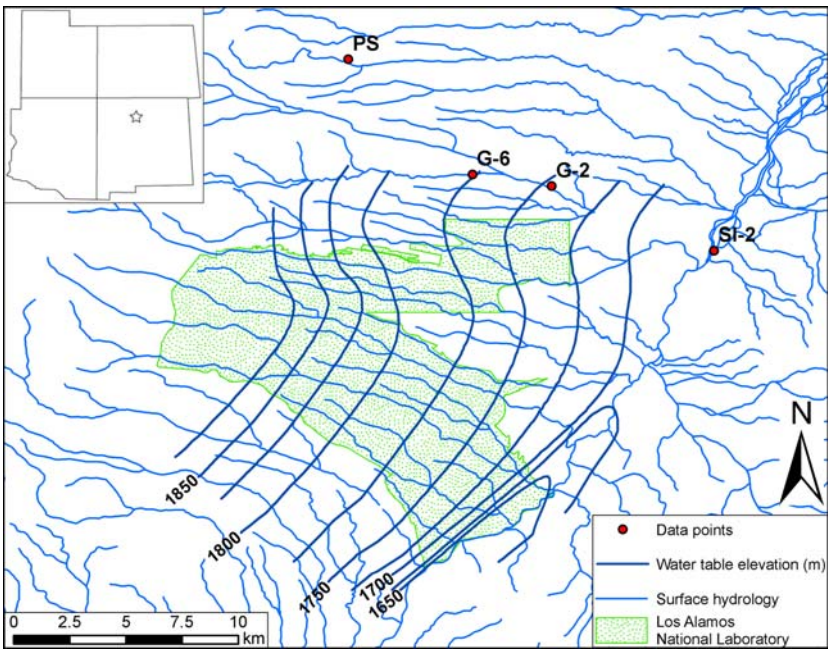

Fig. 1 Hydrologic map of the Pajarito Plateau. Inset shows the four-corners region with the location of the large map marked with a star

and chemical constituents are presented in Table 1 and Fig. 2. The chemical changes along the flow path are representative of the regional trends on the plateau. Generally, the water chemistry changes from calcic-bicarbonate- to sodic-type from west to east. Calcium and magnesium concentrations decrease as sodium concentrations increase. Potassium concentrations decrease along the flow path, ending with a very low concentration (~0.015 mmol/L) near the discharge point. Sulfate concentrations initially decrease slightly, remain unchanged in the second segment, and increase by a factor of more than 30 in the last segment. Chloride concentrations steadily increase along the flow path in conjunction with TDS. These trends are generally consistent with the regional trends in the aquifer, suggesting that the reactions taking place here are representative of those throughout the region.

Three possible hypotheses may explain the major ion geochemical evolution trends observed in the regional aquifer. First, when groundwater is at equilibrium with aquifer minerals but crosses different mineralogical zones in the aquifer, different water chemistry along the flow path may reflect exposure to a new suite of minerals. Second, in a mineralogically homogeneous aquifer, the chemical evolution may be a result of kinetically limited dissolution/precipitation reactions. Third, mixing occurs between waters originating from different regions with different water chemistry. The following model results provide an opportunity to test these hypotheses.

Table 1 Water chemistry along the flow path

	PS	G-6	G-2	SI-2
Sample date	14 May 1991	18 August 1992	18 August 1992	12 May 1993
PH	5.5	8	8.3	9.1
Temp (°C)	12.6	30.3	29.6	14.4
TDS (mg/kg)	126	186.9	233.9	329.5
SiO_2 (mmol/kg)	0.416	0.859	1.187	0.022
Ca^{2+} (mmol/kg)	0.267	0.334	0.239	0.070
Mg^{2+} (mmol/kg)	0.146	0.079	0.021	0.007
Na^{+} (mmol/kg)	0.278	0.809	1.696	4.093
K^{+} (mmol/kg)	0.092	0.063	0.073	0.022
HCO_3^{-} (mmol/kg)	1.000	1.508	1.672	3.097
SO_4^{2-} (mmol/kg)	0.080	0.030	0.040	0.145
Cl^{-} (mmol/kg)	0.041	0.054	0.064	0.096
CO_3 (mmol/kg)	0.000	0.000	0.000	0.375
^{14}C age (ka)	0	6.1	10	32

Data from Blake et al. (1995)

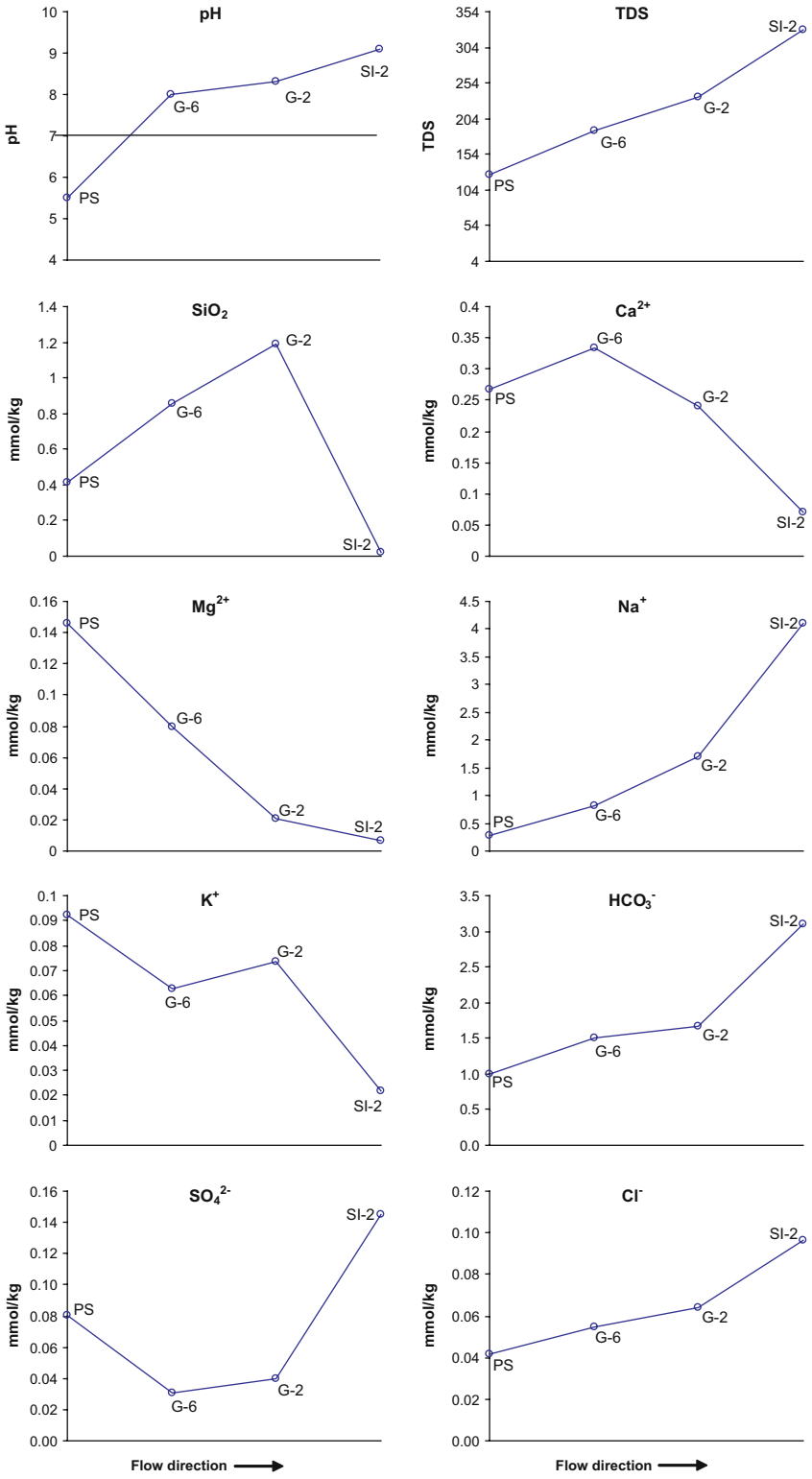

Fig. 2 Chemical evolution along the flow path

Methods

Method of rate estimation

The dissolution rate, r_j (mol s^{-1} m^{-2}), for a mineral, j, can be calculated from

$$r_j = \frac{M_j}{\Delta t}\frac{1}{S_j} \quad (1)$$

where M_j denotes moles of mineral j reacted, Δt the time span over which the reaction occurs, and S_j the mineral surface area. M_j can be calculated using mass-balance relationships to deduce the weathering reactions from changes in the water chemistry, as first proposed by Garrels and Mackenzie (1967).

Inverse mass-balance modeling was used to estimate mass transfer, M_j, along the flow path depicted in Fig. 1. The modeling was conducted with the computer program PHREEQC (Parkhurst and Appelo 1999). PHREEQC calculates possible combinations of mass transfer reactions to match the observed chemical changes of the aqueous solution using input chemical data of the initial and final waters. PHREEQC requires the user to specify mineral phases (both reactants and products), which might participate in the reactions.

Inverse mass-balance modeling employs several assumptions: (a) the initial and final waters are along the same flow path; (b) dispersion and diffusion have a negligible effect on water chemistry; (c) the system has been in a chemical steady state; (d) mineral phases used in the calculations are present in the aquifer (Plummer 1984, 1994,2005; Zhu and Anderson 2002). As true for all inverse methods, inverse mass balance models produce non-unique solutions—that is, several mass transfer models can equally explain the observed chemical changes in the two wells. To reduce the non-uniqueness, SEM, XRD, and petrographic studies were conducted to identify those phases that predominate in the aquifer.

Water sample ages in Table 1 were estimated by overlaying ^{14}C age contours from Rogers et al. (1996) on a map of the area, including well locations, in ArcView GIS. The times, Δt, represent the travel time between wells (the difference between the ^{14}C ages) and have a higher accuracy than the ages themselves (Zhu and Murphy 2000). The surface area term, S_j, in Eq. (1) was estimated from the mineral abundance, porosity, and grain size in core samples (see Appendix).

Petrographic studies

Scanning electron microscopy (SEM) of drill-cuttings and outcrop samples was conducted on a Philips XL 30 field emission gun (FEG) SEM. These studies were critical in (a) identifying mineral phases in the aquifer, (b) recognizing the minerals' textural relationships, which offer evidence of dissolution and precipitation reactions; and (c) estimating surface areas for use in rate calculations. The SEM has secondary electron and back-scattered electron detectors for imaging, as well as an Energy dispersive X-ray spectrometer with an EDAX ultrathin window CDU LEAP detector capable of analyzing light elements down to carbon. Drill cutting samples from the Otowi-1 and R-5 wells in the Santa Fe Group were mixed with epoxy, secured into 2.5 cm phenol rings and gently polished to a smooth, flat surface. Cuttings were also made into double-sided, polished petrographic thin sections. These samples were coated with a layer of carbon before SEM analysis. A large number of electron micrographs were taken with a R. J. Lee Personal SEM.

Estimates of grain size were derived from images of the samples of the Tesuque formation and other unclassified Santa Fe Group rocks. Mineral phase identification was aided with EDAX images. Chemical element maps (Si, Al, K, Na, Ca, and Mg) of electron micrographs allowed for the identification of K-feldspar, plagioclase and quartz grains, which are most abundant in the samples.

Bulk feldspar abundance was calculated by averaging abundance for each formation (Keating and Warren 1999) using only data below the water table, based on the assumption that since local recharge is minimal, the bulk of the reactions take place at or below the water table; the average was weighted based on how much of each formation was below the water table within the screened interval of the well. Composition of feldspars was determined, and feldspar abundance confirmed using EDAX images. EDAX was used to show the distribution of element constituents (Si, Al, K, Na, Ca, and Mg) allowing for the identification and abundance calculation of K-feldspar, plagioclase and quartz grains. Geometric surface areas of feldspars were estimated using grain size and mineral abundance data obtained in this study, and the porosity of these aquifers is estimated to be 25%.

Model construction

A total of eight components (S, Si, Mg^{2+}, Ca^{2+}, K^+, Na^+, Cl^-, and C) were included in the model; ten phases were included (calcite, gypsum, kaolinite, halite, Na–Ca exchange, illite, plagioclase (An38), Ca-montmorillonite, chalcedony and K-feldspar). As the number of phases exceeds the number of components and as not all phases must be included in the final

model, many models are possible. To counter this problem, the program was constrained to only precipitate some phases while only dissolving others, thus reducing the number of models. Precipitation/dissolution constraints were based on mineralogic data and low-temperature kinetics. Low-temperature kinetics suggests the dissolution of feldspars and halite; coatings on mineral grains are evidence of precipitation of clay minerals. Constraints and analytical uncertainties for the models are shown in Table 2. The presence of phases was confirmed with SEM and electron microprobe analysis.

Results

Reactions in the aquifer

The electron microscopy results of a drill cutting from the Otowi-1 well show that all sediment grains have a continuous layer of coating materials a few microns in thickness (Fig. 3). K-feldspar grains are coated with a layer of clayey materials of variable thickness (Figs. 3, 4). Energy dispersive spectra show that the coating materials contain Si, Al, Mg, Ca, and Fe (Fig. 4), resembling the composition of illite/smectite. At 50,000× magnification, the coating materials appear to be crystalline, platy and less than 100 nanometers in size (Fig. 3). Note also in Fig. 3, there is a gap between the coating layer and the feldspar, which is most likely caused during the thin sectioning. However, it illustrates that clay particles do not have epitaxial growth. Interestingly, not only K-feldspar grains are coated. Quartz grains, which are far more abundant than K-feldspar grains, also are coated with clayey materials (Figs. 3, 5). Moreover, small amounts of titanium-iron oxides were found in the samples, which also are coated with a layer of clayey materials (Fig. 5). The presence of a coating on all sediment grains, regardless of grain composition, raises questions about the origin of the coating. Drilling mud was used when the samples were taken. However, the textures show that the clay minerals are unlikely to be drilling mud left in the samples. The clay coatings have nearly constant thickness and no clay particles were found in the interstices. Additionally, the clay coatings in the Santa Fe group resemble those in the Navajo Sandstone outcrop samples at Black Mesa, Arizona (Zhu 2005) and in the Atlantic Coastal Plain sediment outcrop samples, at East Shore of Virginia (Penn et al. 2001), neither of which involves any drilling mud.

Plummer et al. (2004) report that in the Middle Rio Grande Basin (MRGB), which is stratigraphically similar to the Española Basin, vertical variation in aquifer chemistry is smaller and less predictable than horizontal variation. Plummer et al. (2004) note that at shallow depths, water chemistry is more likely to be affected by land use and evapotranspiration. Vegetation and microbes can also play a role in the weathering process. Due to the depth of this aquifer and the arid climate, these factors are relatively insignificant in terms of major ion chemistry of the aquifer waters; here, aquifer chemistry is dominated by mineral weathering reactions.

Figure 6 shows modeled precipitation and dissolution patterns that are generally consistent with mineral phases present. The bulk of the mass transfer for most minerals occurs during the first segment. (It should be noted that this segment differs from the other two in that it includes travel through the vadose zone.) Kaolinite and chalcedony are notable exceptions to this trend. The geochemical reaction models indicate that dissolution of kaolinite, plagioclase and chalcedony, and precipitation of smectite are the dominant groundwater reactions affecting water chemistry in the Santa Fe aquifer.

Shown in Table 3 and Fig. 6 are the models PHREEQC produced for the three segments of the flow path based on the constraints (Table 2). Three possible mass transfer models were found for the first segment of the flow path, Pine Spring (PS) to Guaje-6 (G-6). Model 2 predicts dissolution of K-feldspar, plagioclase and halite; precipitation of chalcedony, calcite, kaolinite, gypsum and illite; and Ca for Na ion exchange. Model 1 differs in that it predicts the dissolution of

Table 2 Model specifications for the three segments of the flow path

	Segment 1: PS-G6	Segment 2: G6-G2	Segment 3: G2-SI2
Uncertainty[a]:			
Solution 1	0.1	0.07	0.1
Solution 2	0.1	0.11	0.11
Forced dissolution	K-feldspar, An38	K-feldspar, An38, Halite	K-feldspar, An38, Halite
Forced precipitation	Ca-montmorillonite	Ca-montmorillonite, Illite, CaX_2	

[a] Uncertainty reported as a fraction of the input value

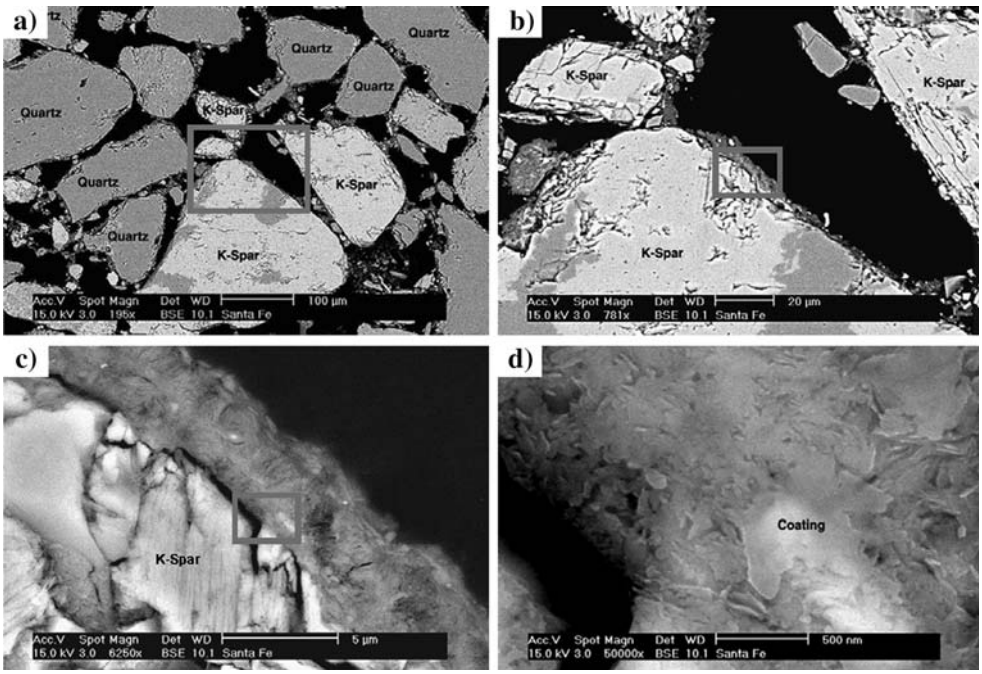

Fig. 3 Clay coatings on a K-feldspar grain. Zoom level increases from (a) to (d). *Rectangles* show the area of the successive images

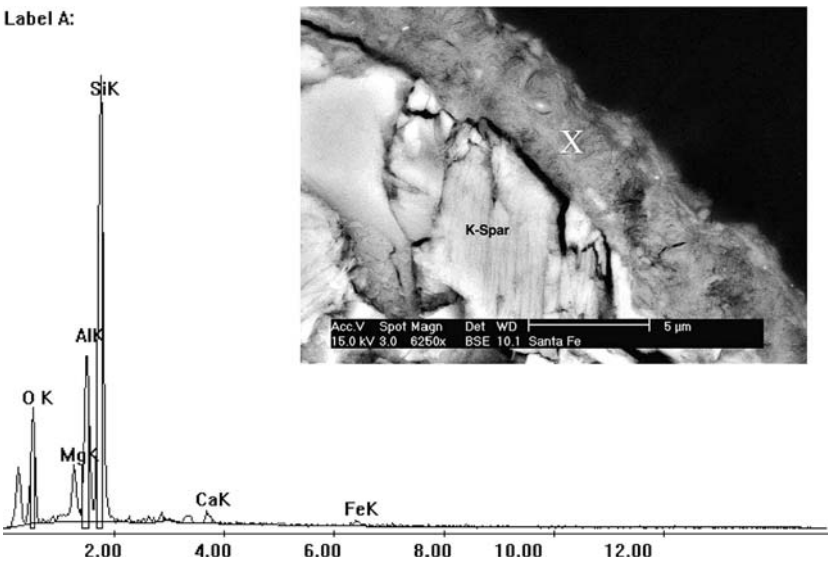

Fig. 4 Enlarged electron scanning micrograph of the clayey coating on a feldspar grain and the EDS spectrum of the coating. (The ''*X*'' marks the spot where the data were collected)

kaolinite instead of precipitation, and the simultaneous precipitation of illite and Ca-montmorillonite. Model 3 also predicts simultaneous precipitation of illite and Ca-montmorillonite, but kaolinite is absent. Model 2 was preferred because it requires precipitation of only one clay mineral rather than two.

The predicted feldspar dissolution and clay precipitation appear to be consistent with petrographic observations discussed above. The mass transfer model requires precipitation of gypsum and calcite to account for the decrease of sulfate and total dissolved inorganic carbon from PS to G-6. This contradicts the saturation index calculations (Fig. 7). One possibility is error in the analytical data—alkalinity measurements and reporting are often problematic (Zhu and Anderson 2002). Another possibility is that the ''net reaction'' along the flow path between PS and G-6 is the precipitation of gypsum and calcite, although locally at PS and G-6 calcite and gypsum are under-saturated. This hypothesis is supported by Plummer et al. (2004), who note the presence of calcite cement in the Santa Fe aquifer, especially at depth. Because there are no Al measurements, saturation indices for aluminosilicates were not computed.

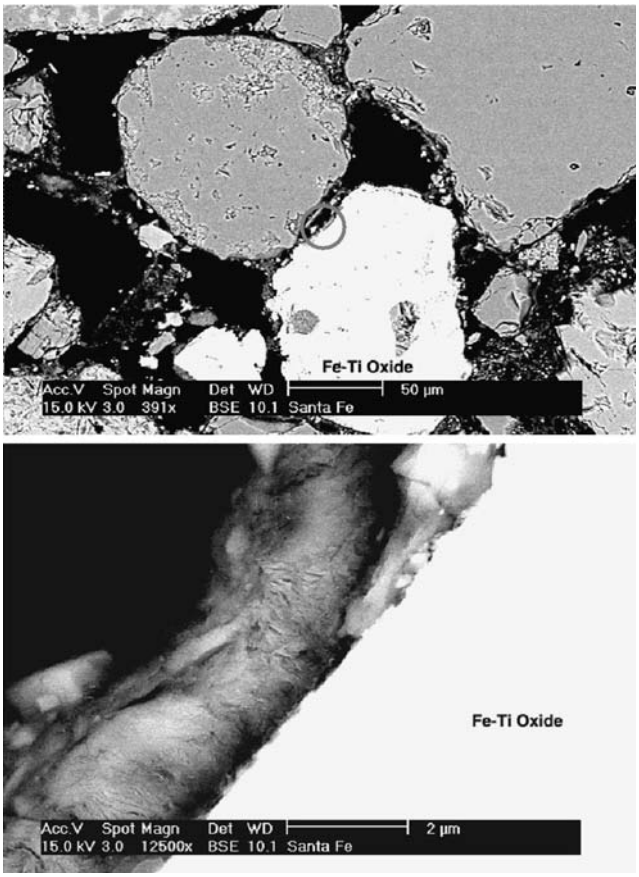

Fig. 5 Clay coatings on Fe-Ti oxide grains

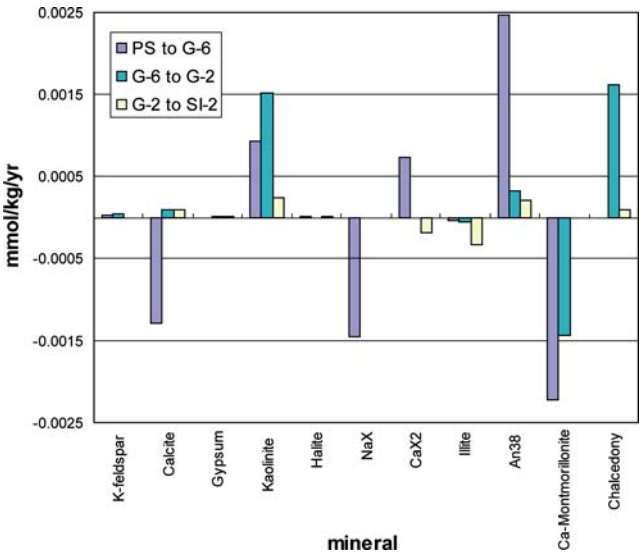

Fig. 6 Mass transfer for different segments of the flow path

From G-6 to G-2, a total of five mass transfer models were computed to account for the chemical evolution. All five models are quite similar. Model 5 was preferred because it uses the minimum number of phases. Model 5 predicted the dissolution of K-feldspar, plagioclase, gypsum, calcite, kaolinite and chalcedony; and precipitation of illite and Ca-montmorillonite.

From G-2 to SI-2, six models fit the chemical evolution along the path. Model 6 was eliminated due to exceptionally high rates of kaolinite dissolution and illite precipitation. Model 4 predicts the dissolution of calcite, gypsum, kaolinite, halite and plagioclase; and precipitation of illite and chalcedony, with Ca for K and Mg ion-exchange. The analytical data show a large drop of $SiO_{2(aq)}$ from G-2 (71.3 mg/L) to SI-2 (1.3 mg/L). Other wells near SI-2 typically have a $SiO_{2(aq)}$ concentration of ~30 mg/L which still represents a significant decline from the previous well in the flow path. Using a value of 30 mg/L would generate similar models in terms of phases involved, but different mass transfer rates. There is more uncertainty inherent in this segment of the flow path due to the atypical Si data.

Mineral dissolution and precipitation rates

Using the results from inverse mass balance modeling and travel times estimated from ^{14}C data, reaction rates were calculated. Table 4 shows the dissolution and precipitation rates for K-feldspar, plagioclase, illite, Ca-montmorillonite, calcite, gypsum, and chalcedony. These rates are apparent rates in mol L^{-1} s^{-1}.

To compare these rates to other aquifers, it was necessary to normalize the rates with respect to surface area. As described above, the petrographic studies allowed for an estimate of geometric surface areas based on grain size, mineralogical abundances, and porosity estimates. Table 5 shows the calculated rates based on geometric surface areas of approximately 0.02 m^2/g. Geometric surface areas were derived from feldspar density values and average grain size as measured on SEM images. The dissolution rate ranges from $10^{-14.6}$ to $10^{-15.4}$ mol (feldspar) m^{-2} s^{-1} for plagioclase, and $10^{-16.6}$ to $10^{-16.8}$ mol (feldspar) m^{-2} s^{-1} for K-feldspar (Table 5). Plagioclase dissolution occurs at a rate one to two orders of magnitude faster than K-feldspar dissolution, which is consistent with other field studies (White et al. 2001).

One large uncertainty in deriving feldspar reaction rates is in the estimation of reactive surface area. There are three methods commonly used for describing the surface area of silicate minerals for reaction kinetics: geometric, BET, and reactive surface area. ''Reactive'' surface area is an insightful concept (Helgeson et al. 1984), but, at present, is too poorly defined to be quantitatively useful. BET surface area (based on the volume of gas, usually N_2 or Kr, adsorbed on the sample surface) is the most useful measure of the

Table 3 Mass transfer models suggested by PHREEQC

Phase	Model 1	Model 2	Model 3
(a) PS to G-6			
K-feldspar	**1.31E-04**	1.31E-04	1.31E-04
Calcite	**–7.81E-03**	–7.81E-03	–7.81E-03
Gypsum	**–4.97E-05**	–4.97E-05	–4.97E-05
Kaolinite	**5.64E-03**	–7.90E-03	
Halite	**1.30E-05**	1.30E-05	1.30E-05
NaX	**–8.88E-03**	–6.88E-03	–8.05E-03
CaX_2	**4.44E-03**	3.44E-03	4.02E-03
Illite	**–2.67E-04**	–2.67E-04	–2.67E-04
An-38	**1.50E-02**	1.18E-02	1.37E-02
Ca-Montmorillonite	**–1.35E-02**		–7.90E-03
Chalcedony		–1.41E-02	–5.89E-03

Phase	Model 1	Model 2	Model 3	Model 4	Model 5
(b) G-6 to G-2					
K-feldspar	1.52E-04	1.52E-04	1.62E-04	1.52E-04	**1.52E-04**
Calcite	3.29E-04	3.33E-04	2.03E-04	3.29E-04	**3.33E-04**
Gypsum	9.06E-06	9.06E-06	1.34E-05	9.06E-06	**9.06E-06**
Kaolinite	7.85E-04	7.89E-04	2.25E-04	5.83E-03	**5.90E-03**
Halite	9.87E-06		1.57E-05	9.87E-06	
NaX	7.48E-04	7.57E-04	6.74E-04		
CaX_2	–3.74E-04	–3.79E-04	–3.37E-04		
Illite	–2.35E-04	–2.35E-04	–2.67E-04	–2.35E-04	**–2.35E-04**
An-38				1.21E-03	**1.22E-03**
Ca-Montmorillonite	–5.07E-04	–5.10E-04		–5.55E-03	**–5.62E-03**
Chalcedony	9.86E-04	9.90E-04	3.23E-04	6.25E-03	**6.32E-03**

Phase	Model 1	Model 2	Model 3	Model 4	Model 5	Model 6
(c) G-2 to SI-2						
K-feldspar		9.27E-04	2.10E-03		2.26E-03	9.64E-03
Calcite	2.02E-03	2.02E-03	2.02E-03	**2.02E-03**	2.02E-03	2.02E-03
Gypsum	1.05E-04	1.05E-04	1.05E-04	**1.05E-04**	1.05E-04	1.05E-04
Kaolinite	1.92E-03	2.43E-03	3.07E-03	**5.35E-03**	6.58E-03	1.06E-02
Halite	3.19E-05	3.19E-05	3.19E-05	**3.19E-05**	3.19E-05	3.19E-05
NaX	2.82E-03	2.82E-03	2.82E-03			
CaX_2	–2.29E-03	–2.29E-03	–2.29E-03	**–4.02E-03**	–4.02E-03	–4.02E-03
KX	9.52E-04	5.31E-04		**4.38E-03**	3.35E-03	
MgX_2	4.05E-04	6.15E-04	8.81E-04	**1.83E-03**	2.35E-03	4.02E-03
Illite	–1.67E-03	–2.52E-03	–3.58E-03	**–7.39E-03**	–9.44E-03	–1.62E-02
An-38				**4.55E-03**	4.55E-03	4.55E-03
Chalcedony	8.43E-04		–1.06E-03	**2.05E-03**		–6.71E-03

Units are mol/L. Preferred models are in bold type

mineral surface exposed to solution for reaction (Blum 1994), and is also the most comparable with previous studies. However, the paucity of samples in this study precludes BET surface area measurement. In this study, geometric surface areas were computed from an assumed grain shape and size distribution. The ratio of BET/geometric surfaces is known as the ''surface roughness'' (SR) (Helgeson et al. 1984), but also includes internal porosity. Blum (1994) compiled the SR of ground experimental materials (which are usually museum-grade mineral samples) to be 8.5 ± 5, which thus represents a minimum value for natural minerals. The SR of naturally weathered feldspars varies from ~250 to 3,000 (White and Peterson 1990; Blum 1994; White et al. 1996), with the SR increasing systematically with the qualitative degree of corrosion and internal porosity development (White et al. 1996; White and Brantley 2003). Therefore, as these calculations do not consider SR, they overestimate dissolution rates. It should be kept in mind that geometric surface area estimates may fall short of the actual physical surface area by one to two orders of magnitude; the physical surface area is, however, often an overestimate for the reactive surface area because of

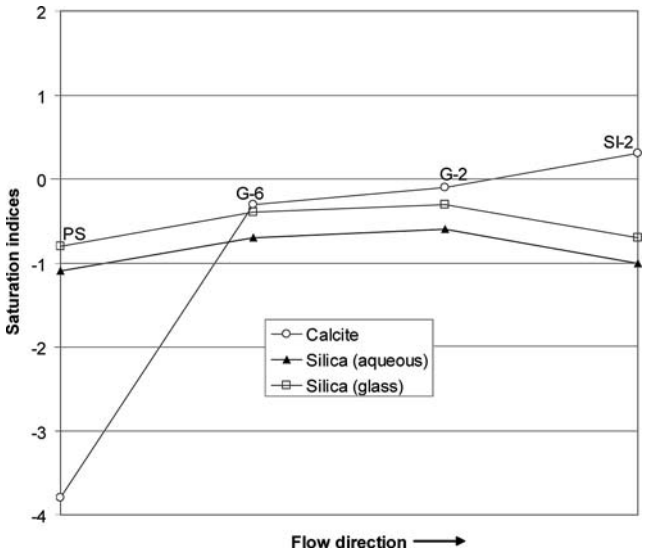

Fig. 7 Saturation indices for selected minerals

Table 4 Mineral reaction rates

	Rate (mol L^{-1} s^{-1} × 10^{-15})		
	PS-G6	G6-G2	G2-SI2
K-feldspar	0.68	1.23	
An-38	78.13	9.93	6.56
Illite	–1.38	–1.91	–10.64
Ca-Montmorillonite	–70.34	–45.65	
Chalcedony		51.36	2.95
Calcite	–40.56	2.70	2.91
Gypsum	–0.26	0.07	0.15

Positive values indicate dissolution; negative values indicate precipitation

Table 5 Calculated feldspar dissolution rates, normalized to surface area

	Rate (mol m^{-2} s^{-1} × 10^{-15})
K-feldspar	
PS-G6	0.015 ± 0.0095
G6-G2	0.027 ± 0.020
G2-SI2	
An-38	
PS-G6	2.8 ± 1.7
G6-G2	0.43 ± 0.32
G2-SI2	0.35 ± 0.19

clay coatings on grains (White and Peterson 1990; Rowe and Brantley 1993).

To assess the uncertainties in porosity, mineral abundance, and ^{14}C based travel time, an error propagation analysis was performed and is described in the appendix. All errors were found to be the same or smaller order of magnitude than the rate estimate.

Few experimental data are available for dissolution rates of feldspars at near neutral pH (see review by Blum and Stillings 1995). At 25°C and ''basic pH'', the laboratory dissolution rate for K-feldspar, mostly from Schweda (1989, 1990), is $10^{-12.5}$ mol m^{-2} s^{-1}. Plagioclase dissolution rates are a function of Ca/Na ratios, but most plagioclase rates are skewed toward the albite end. For an An–38 plagioclase, the dissolution rate at pH 5.0 is about $10^{-11.5}$ mol m^{-2} s^{-1} (Fig. 5 of Blum and Stillings 1995). Thus, the in situ dissolution rates in this regional aquifer appear to be about 10^5 times slower than the laboratory rates at similar pH and temperature, in the absence of further qualifications of other conditions (e.g., chemical affinity). This discrepancy is even larger than that found in soil and watershed studies, where field rates are a factor of 10^2–10^4 slower than those measured in the laboratory. However, these reaction rates are comparable to other deep aquifer studies (Zhu 2005).

Discussion of model assumptions

Inverse mass-balance modeling is based on several fundamental assumptions; the results of reaction rates presented above must be viewed in this context. Assumption 1: the initial and final waters are along the same flow path. Given the scale of the study, it is impossible to delineate the precise flow path of a distinct parcel of water. Therefore, the sample locations used for the model were selected as representative of general flow direction in the region. The flow path was constructed perpendicular to the water table contours, and the wells were chosen so that the changing water chemistry represents the regional trend of chemical evolution. Some of the wells in the Pajarito Plateau are screened over large intervals (up to 300–600 m), resulting in a mix of waters, which renders saturation index calculations ambiguous and reinforces the notion that the regional trends are more important.

It has been suggested that local recharge in the vicinity of the Rio Grande could be a source of young water mixed into the deep wells (Keating and Warren 1999). While some data (TDS and pH, along with internally consistent calculated reaction rates) indicate a lack of significant mixing with younger waters in the SI–2 well (the only sample location near the Rio Grande), other data (an unexplained sharp increase in SO_4^{2-} and decrease in SiO_2 along this last segment) support the possibility of mixing.

Assumption 2: dispersion and diffusion have, at most, a negligible effect on water chemistry. This is an assumption that is difficult to assess without detailed knowledge of the aquifer's hydraulic properties. Thus

the calculated rates are effective rates that may have inherited the hydraulic properties and structures of the aquifer. The large size of the aquifer, time scale of flow, and large screening interval of the wells contribute to making this a reasonable assumption.

Assumption 3: the system operates in a chemical steady state. Changes in input water can cause misinterpretation of the data (as far as which reactions are taking place). Dramatic climate shifts have affected the US southwest during the past several thousand years, causing recharge rates to fluctuate by a factor of two to three (Ortega-Ramirez et al. 1998; Zhu et al. 1998; Polyak et al. 2004) but no reports were found of chemical changes to recharge waters during this time frame. Anthropogenic effects have been registered at some wells on the plateau, including elevated ^{3}H at Otowi-1 (Keating et al. 2005) and while the majority of recharge to the aquifer continues to occur west and up gradient of LANL, the effects of the waste produced at LANL cannot be dismissed.

Assumption 4: mineral phases used in the calculations are present in the aquifer. Inverse models produce non-unique solutions. Although extensive petrographic identifications were conducted, it is difficult to ascertain the relationships between water chemistry and observed mineral alterations.

While studying reaction rates in aquifer systems in situ may seem tedious and impractical, at this time it seems to be one of the most reliable means to produce an accurate estimate. Rates derived from soil profile and surface water systems are usually not applicable to aquifer systems due to differences between saturated and unsaturated systems (wetted vs. unwetted mineral surface area, biochemical effects which vary with depth and degree of saturation, migrating saturated zones associated with shallow systems).

Conclusions

The pronounced chemical evolution from recharge to discharge observed in the regional aquifer on the Pajarito Plateau can be explained by kinetically controlled chemical reactions. No evidence of coincidental mineralogical zonation was found. The inverse mass-balance method was used to model these reactions, which were supported by SEM and XRD data. Dissolution of K-feldspar, plagioclase, kaolinite, halite and chalcedony; precipitation of illite and/or Ca-montmorillonite; and Ca–Na–K–Mg ion exchange reactions are predicted. Calcite and gypsum are predicted to dissolve along the first segment of the flow path and precipitate for the balance of the flow path.

The inverse modeling results, in combination with geometric surface area estimates and ^{14}C data were used to calculate reaction rates. It is important to remember that inverse models offer non-unique solutions and also that there is a degree of uncertainty associated with ^{14}C ages and geometric surface area estimates. The estimated rate at which plagioclase feldspar dissolution is taking place is on the order of 10^{-15} mol m^{-2} s^{-1}; the corresponding rate for potassium feldspar dissolution is 10^{-17} mol m^{-2} s^{-1}. These rates are several orders of magnitude slower than laboratory experimental rates.

While no two aquifer systems are identical, the reactions and reaction rates determined for the Santa Fe aquifer certainly hold implications for other sandstone aquifers in arid regions. As more aquifers are evaluated in this manner, it will become evident which aspects of an aquifer system are most influential in terms of controlling reactions and reaction rates, and possible to simulate these conditions in laboratory studies. Understanding the reactions that take place in natural systems will facilitate more accurate modeling of processes such as contaminant transport, soil development and the global carbon cycle.

Acknowledgments This work was partially funded by an Institute of Geophysics and Planetary Physics grant (#1208) and two National Science Foundation grants (EAR0423971 and EAR0509775) awarded to CZ. A National Science Foundation grant (#0318769) awarded to Juergen Schieber and four other faculty members and the NSF grant (EAR0423971) to CZ allowed for the purchase of the SEM at Indiana University.

Appendix: Error propagation analysis

Dissolution rates were calculated from the following equation,

$$R_j = \frac{M_j}{\Delta t}\frac{1}{S_j} \tag{2}$$

where M_j denotes moles of mineral j reacted per liter; Δt is the time span over which the reaction occurs (seconds), and S_j the mineral surface area per liter of groundwater (m^2/L). S_j is calculated from the specific surface area (m^2/g), s_j,

$$S_j = \frac{\Psi_j 10^3 \rho_j s_j}{\theta} \tag{3}$$

where Ψ and ρ denote the volumetric abundance of *jth* feldspar (%) and mineral particle density (g/cm^3), respectively. θ stands for the porosity of the aquifer. Combining Eqs. (2) and (3),

$$R_j = \frac{M_j}{\Delta t}\frac{\theta}{\Psi_j 10^3 \rho_j s_j}. \quad (4)$$

Using the error propagation equation from Anderson (1976), the uncertainty of calculated dissolution rates resulting from uncertainty in individual parameters used in the calculation can be computed as follows, if all of the variables are statistically independent,

$$\sigma^2_{R_+} = \left\{\frac{\theta}{\Delta t \Psi_j 10^3 \rho_j s_j}\right\}^2 \sigma^2_{M_j} + \left\{-\frac{M_j \theta}{\Delta t^2 \Psi_j 10^3 \rho_j s_j}\right\}^2 \sigma^2_{\Delta t} + \left\{\frac{M_j}{\Delta t \Psi_j 10^3 \rho_j s_j}\right\}^2 \sigma^2_{\theta} + \left\{-\frac{M_j \theta}{\Delta t \Psi_j^2 10^3 \rho_j s_j}\right\}^2 \sigma^2_{\Psi} + \left\{-\frac{M_j \theta}{\Delta t \Psi_j 10^3 \rho_j s_j^2}\right\}^2 \sigma^2_{s_j}.$$

An effective porosity of 25% was assumed with variation ±5%. Feldspar abundance was estimated from optical microscopy, XRD and SEM studies. One-third of the feldspar was assumed to be plagioclases and two-thirds to be K-feldspar. An error of ±40% of the abundance value was used for K-feldspar and plagioclase variation. However, this study area covers over 800 km^2 and spatial heterogeneities of effective porosity and feldspar abundances are difficult to estimate. Travel time was constrained from radiocarbon ages, assuming an error of ±2,000 years. M_j is a modeling result. An exact value is difficult to assess, but an error of ±10% was assumed. Specific geometric surface areas were estimated from grain size with an error of ±25%. There are conceptual issues regarding what constitutes ''reactive surface area'' and practical difficulties in estimation and measurements of geometric and BET surface areas, which are difficult to evaluate. See the text for more discussion.

The results show errors (σ) are of the same order of magnitude as the rates, or ±53–73%. Among the parameters for surface area calculations, porosity and mass transfer consistently make the smallest contribution to error. The errors in mineral abundance (±40%) and in groundwater travel time (±2,000 years) have the largest impact on the combined error.

However, while a formal error propagation analysis is meaningful to analyze the relative contributions of variables in the rate estimates, the error bars should not be construed as a reassurance. The fundamental question remains what is the relationship between geometric surface area and ''effective reactive surface area.'' Inverse mass balance interpretations of solute fluxes are non-unique, which leads to the difficulty of assigning an error to M_j.

References

Alsaaran N, Olyphant GA (1998) A model for simulating rock–water interactions in a weathering profile subjected to frequent alternations of wetting and drying. Catena 32:225–243

Anderson GM (1976) Error propagation by the Monte Carlo method in geochemical calculations. Geochim Cosmochim Acta 40:1533–1538

Blake WD, Goff F, Adams AI, Counce D (1995) Environmental geochemistry for surface and subsurface waters in the Pajarito Plateau and outlying areas, New Mexico. Los Alamos Natl Lab report LA-12912–MS

Blum AE (1994) Feldspars in weathering. In: Parsons I (ed) Feldspars and their reactions. Kluwer, Dordrecht, pp 595–629

Blum AE, Stillings LL (1995) Feldspar dissolution kinetics. In: White AF, Brantley SL (eds) Chemical weathering rates of silicate minerals.Reviews in Mineralogy, Mineralogical society of America, pp 291–346

Brantley SL (1992) Kinetics of dissolution and precipitation-experimental and field results. Proceedings of the seventh international conference on water–rock interactions, Utah, pp 465–469

Broxton DE, Vaniman DT (2005) Geologic framework of a groundwater system on the margin of a rift basin, Pajarito Plateau, north-central New Mexico. Vadose Zone J 4:522–550

Drever JI, Clow DW (1995) Weathering rates in catchments. In: White AF, Brantley SL (eds) Chemical weathering rates of silicate minerals. Reviews in mineralogy, Mineralogical society of America, pp 463–481

Frenzel PF (1995) Geohydrology and simulation of ground water flow near Los Alamos, north-central New Mexico. USGS water-resources investigation, pp 95–1049

Garrels RM, Mackenzie FT (1967) Origin of the chemical composition of some springs and lakes. In: Stumm W (ed) Equilibrium concepts in natural water systems.American chemical society advances in chemistry series, American chemical society, pp 222–242

Griggs RL (1964) Geology and ground water resources of the Los Alamos area, New Mexico. USGS water supply paper, pp 1753

Helgeson HC, Murphy WM, Aagaard P (1984) Thermodynamic and kinetic constraints on reaction rates among minerals and aqueous solutions II. Rate constants,effective surface area, and the hydrolysis of feldspar. Geochim Cosmochim Acta 48:2405–2432

Keating EH, Bahr JM (1998) Using reactive solutes to constrain groundwater flow models at a site in northern Wisconsin. Water Resour Res 34:3561–3571

Keating E, Warren R (1999) Geochemistry of the regional aquifer: internal report, environmental restoration program, Los Alamos National Laboratory, 35pp

Keating EH, Robinson BA, Vesselinov VV (2005) Development and application of numerical models to estimate fluxes through the regional aquifer beneath the Pajarito Plateau. Vadose Zone J 4:653–671

McAda DP, Wasiolek M (1988) Simulation of the regional geohydrology of the Tesuque aquifer system near Santa Fe, New Mexico. USGS water-resources investigation, pp 87–4056

Newman BD, Robinson BA (2005) The hydrogeology of Los Alamos National Laboratory: site history and overview of vadose zone and groundwater issues. Vadose Zone J 4:614–619

Ortega-Ramirez JR, Valiente-Banuet A, Urrutia-Fucugauchi J, Mortera-Gutierrez CA, Alvarado-Valdez G (1998) Paleoclimatic changes during the Late Pleistocene-Holocene in Laguna Babicora, near the Chihuahuan Desert, Mexico. Can J Earth Sci 35:1168–1179

Paces T (1983) Rate constants of dissolution derived from the measurements of mass balance in hydrological catchments. Geochim Cosmochim Acta 37:1855–1863

Parkhurst DL, Appelo CAJ (1999) User's guide to PHREEQC (version 2)—a computer program for speciation, batch-reaction, one-dimensional transport, and inverse geochemical calculations. Water resources investigations, pp 99–4259

Penn RL, Zhu C, Xu H, Veblen DR (2001) Iron oxide coatings on sand grains from the Atlantic coastal plain: HRTEM characterization. Geology 29:843–846

Plummer LN (1984) Geochemical modeling: a comparison of forward and inverse methods. In: Hitchon B, Wallick EI (eds) First Canadian/American conference on hydrogeology, practical applications of ground water geochemistry. National water well association

Plummer LN (2005) Retrieval of rates of mineral–water reactions from groundwater systems. GSA annual meeting and exposition abstracts with programs. Geol Soc Am

Plummer LN, Back WW (1980) The mass balance approach—application to interpreting the chemical evolution of hydrologic systems. Am J Sci 280:130–142

Plummer LN, Parkurst DL, Thorstenson DC (1983) Development of reaction models for groundwater systems. Geochim Cosmochim Acta 47:665–685

Plummer LN, Prestemon EC, Parkhurst DL (1994) An interactive code (NETPATH) for modeling NET geochemical reactions along a flow PATH—version 2.0. USGS water-resources investigation, pp 94–4109

Plummer LN, Bexfield LM, Anderholm SK, Sanford WE, Busenberg E (2004) Geochemical characterization of ground-water flow in the Santa Fe Group aquifer system, Middle Rio Grande Basin, New Mexico. USGS water-resources investigation, pp 03–4131

Polyak VJ, Rasmussen JBT, Asmerom Y (2004) Prolonged wet period in the southwestern United States through the Younger Dryas. Geology 32:5–8

Purtymun WD (1995) Geologic and hydrologic records of observation wells, test holes, test wells, supply wells, springs and surface water stations in the Los Alamos area. LA-12883–MS

Rogers DB, Stoker AR, McLin SG, Gallaher BM (1996) Recharge to the Pajarito Plateau regional aquifer system. New Mexico geological society forty seventh field conference. New Mexico geological society

Rowe G, Brantley SL (1993) Estimation of the dissolution rates of andestic glass, plagioclase, and pyroxene in a flank aquifer of Poas Volcano, Costa Rica. Chem Geol 105:71–88

Schweda P (1989) Kinetics of alkali feldspar dissolution at low temperature. In: Miles DL (ed), Proceedings of the sixth International Symposium on water–rock interaction. A A Balkema, Amsterdam, pp 609–612

Schweda P (1990) Kinetics and mechanisms of alkali feldspar dissolution at low temperatures. PhD, Stockholm University, Sweden

Velbel MA (1985) Geochemical mass balances and weathering rates in forested watersheds of the southern Blue Ridge. Am J Sci 285:904–930

Velbel MA (1990) Influence of temperature and mineral surface characteristics on feldspar weathering rates in natural and artificial systems: a first approximation. Water Resour Res 26:3049–3053

White AF, Brantley SL (2003) The effect of time on the weathering of silicate minerals: why do weathering rates differ in the laboratory and field? Chem Geol 202:479–506

White AF, Peterson ML (1990) Role of reactive-surface-area characterization in geochemical kinetic models, Chemical modeling in aqueous systems II. American Chemical Society, pp 461–475

White AF, Blum AE, Schulz MS, Bullen TD, Harden JW, Peterson ML (1996) Chemical weathering of a soil chronosequence on granite alluvium I. Reaction rates based on changes in soil mineralogy. Geochim Cosmochim Acta 60:2533–2550

White AF, Bullen TD, Schulz MS, Blum AE, Huntington TG, Peters NE (2001) Differential rates of feldspar weathering in granitic regoliths. Geochim Cosmochim Acta 65:847–869

Zhu C (2005) In situ feldspar dissolution rates in an aquifer. Geochim Cosmochim Acta 69:1435–1453

Zhu C, Anderson GM (2002) Environmental applications of geochemical modeling. Cambridge University Press, London

Zhu C, Murphy WM (2000) On radiocarbon dating of ground water. Ground Water 38:802–804

Zhu C, Waddell RK, Star I, Ostrander M (1998) The responses of groundwater in the Black Mesa basin, northeastern Arizona to paleoclimatic changes during late Pleistocene and Holocene. Geology 26:27–130